Mach number effect on the aeroelastic phenomenon of fixed wing aircraft

Marcel Ilie¹ and John Havenar² Georgia Southern University, Statesboro, GA, 30458

The aeroelastic phenomenon plays a critical role in the aerodynamic performance and stability of fixed wing aircrafts. Aeroelastic phenomena may cause flow separation and large deformations of the wing, and implicitly high stresses into the structure. The computational study of aeroelasticity, in high-speed fixed wing, requires fully-coupled aeroelastic algorithms. Therefore, in the present research we propose a CFD based approach using the large-eddy simulation approach along with a finite-element method for the computations of the structural deformations. The analysis is performed for subsonic and transonic flows with Mach number $M=0.1 \div 0.3$. The analysis reveals that the elastic deformations of the wing and stresses in the wing increase with the Mach number.

I. Introduction

Aeroelasticity has become an important phenomena in modern rotary/fixed wing flying vehicle. The importance of the aeroeleasticity steams from the performance and stability of aircraft. It is acknowledged that aeroelastic effects in either rotary or fixed wing aircrafts may pose significant challenges and in case of resonance it may lead to destructive consequences. The aeroleasticity has been studied both, experimentally and computationally. However, there are significant challenges left which require further understanding. One of these changes is associated with the supersonic/hypersonic flights. Experimental studies of aeroelastic phenomena in supersonic/hypersonic flights pose significant challenges due the costly equipment and data accuracy. Therefore, experimental studies of aerolasticity in these kind of flights are cumbersome. The latest developments in the computing power have made the computational studies of aerolastic phenomena more feasible. The aeroelasticity represents basically the interaction between two different media, namely structure and fluid flow. Nowadays, aeroelastic studies are carried out by coupling two different solvers, one for fluid flow and the other one for the structure. Usually the fluid flow is computed using the computational fluid dynamics (CFD), employing either finite-difference of fine-volume approaches. The structure is usually computed using finite element methods. The coupling between the two solvers ensure the full-coupling of the fluid and structure. A data-passing service couples these systems together by sending surface forces from the CFD solver to the FEA solver and returning incremental displacements from the FEA solver to the CFD solver. In order to obtain a robust solution while using a transient simulation approach, a staggered iterative loop may be used. For strongly coupled fluid-structural interaction problems, it is common for the viscous flow regime to be resolved using unsteady Reynolds-average Navier-Stokes (URANS) equations rather than the large eddy simulation (LES), scale adaptive simulation (SAS), and detached eddy simulation (DES) approaches due the high CPU time costs that are incurred when they are paired with a staggered, time-marching approach.

The purpose of this work is to investigate the aeroelastic response of an aircraft wing for varied angles of attack and flow velocities. By observing the induced oscillating stresses and displacements in the structural domain over

¹ Assistant Professor, Department of Mechanical Engineering

² Undergraduate Student, Department of Mechanical Engineering

several angles of attack for various freestream flow velocities, a relationship between the freestream Mach number and the induced aeroelasticity may be characterized. This work also serves reinforce the continually growing body of literature which makes use of commercial CFD and FEA codes for modeling complex, unsteady aeroelastic phenomena.

The main goal of this research is to study the aeroelastic effect on the aerodynamic performance of high-speed fixed wing aircraft. The focus on aerodynamic performance and efficiency of planes and spacecraft have been at the forefront of the aerospace industry since the beginning of its existence. The lift and drag of airfoils have been extensively studied to determine the optimum shape and angle of attack (AoA) to generate sufficient lift. As an airfoil reaches its critical AoA, where lift is maximized, a pressure gradient causes the flow to detach from the surface. The phenomenon known as flow separation occurs causing a decrease in lift and an increase in drag. If the reduction in lift is significant enough, the flow separation may lead to stalling. Occasionally, flow may reattach to the surface and form "short bubbles", however slight variations in orientation or velocity may cause the bubble to contract resulting in complete flow separation. The present studies concerns the effect of the aeroelastic on the flow separation and aerodynamic performance.

II. Computational method and models

The present study used a NACA 0012 airfoil with a chord length of 1 meter and a span of 0.5 meters. The configuration of the airfoil and the domain is shown in Figure 1.

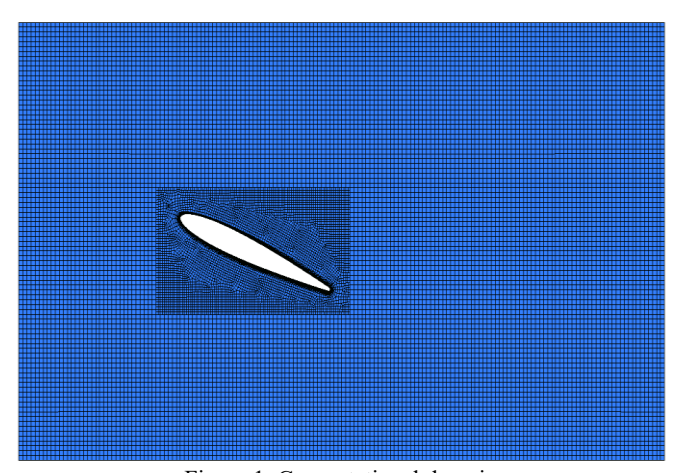


Figure 1. Computational domain

In the present work, a large eddy simulation (LES) approach is used for the computation of the flow field. The 3-D simulations are performed for a wide range of Mach numbers $M=0.1\div 1.2$. The computational domain consists of 4.6 millions grid points, with a cluster of grid points around the airfoil and a grid expansion factor of 0.1. For all the computations in the present analysis, a dimensionless time step $\overline{\Delta t} = \Delta t U_{\infty} / c = 1 \text{x} 10^{-6}$ is chosen, where U_{∞} is the free-stream velocity. The time-step is determined with respect to the explicit time-marching scheme (fourth order Runge-Kutta) and temporal resolution requirement of LES (CFL ≤ 1). The flow field is solved using the filtered Navier-Stokes equations along with a standard subgrid scale (SGS) model and van Driest wall damping. The boundary conditions were assigned as follows. No slip boundary conditions are used at the blades walls. Free slip boundary conditions are used at the top and bottom walls with opening at the end of the computational domain. Periodic boundary conditions are assigned for the lateral surfaces.

The main idea of LES is to separate the flow variable in two components, namely the mean $\overline{f}(x)$ or large scales and fluctuating component f'(x) or small scales. In LES, the large scales of the flow are completely resolved while the small scales are completely modeled using a sub-grid scale model. The governing equations of LES are the so-called filtered Navier-Stokes equations, which are a result of spatial averaging. The filtered Navier-Stokes equations are:

$$\frac{\partial \overline{u_j}}{\partial x_i} = 0 \tag{1}$$

$$\frac{\partial \overline{u_i}}{\partial t} + \frac{\partial \left(\overline{u_i}\overline{u_j}\right)}{\partial x_j} = -\frac{1}{\overline{\rho}} \frac{\partial \overline{p}}{\partial x_i} - v \frac{\partial^2 \overline{u_i}}{\partial x_i \partial x_j} + \frac{\partial \tau_{ij}}{\partial x_i} + S_i$$
(2)

where t is the time, p is the pressure, ρ the density, ν kinematic viscosity, S_i a source term and τ_{ij} the subgrid scale (SGS) tensor expressed as:

$$\tau_{ij} = \overline{u_i} \overline{u_j} - \overline{u_i} \overline{u_j} \tag{3}$$

An eddy viscosity model is used to model the SGS tensor which is then expressed as:

$$\tau_{ij} - \frac{1}{3}\tau_{kk}\delta_{ij} = 2\nu\overline{S_{ij}} \tag{4}$$

where $\overline{S_{ij}}$ is the strain rate based on the filtered velocity $\overline{u_i}$ and ν the eddy viscosity.

In the present work we employ the dynamic Smagorinsky sub-grid scale (SGS) model. The model is presented briefly in the following. In LES, the SGS model represents the effect of small scale (smaller than the grid size Δ) flow structures on the large ones (which are resolved). The large scale flow structures are obtained through a filtering process of the velocity and scalar fields at the grid scale such that

$$\widetilde{u}(x) = \int u(x')F(x-x')dx' \tag{5}$$

where \widetilde{u} is the filtered velocity and F is the filter function at scale Δ .

In 1991 Germano et al., [9], proposed the so-called dynamic Smagorinsky model. In this model the selected features of the resolved scales of the flow field are dynamically analyzed during the simulation, to determine the unknown model coefficient instead of using some predefined values. One fundamental characteristic of the dynamic Smagorinsky SGS model is that the resolved scales can represent much better the flow dynamics phenomena such as stratification, coherent structures and complex flow interactions compared with other turbulence models. The dynamic Smagorinsky SGS model is based on the Germano identity given by:

$$L_{ij} = \overline{\widetilde{u}_i \widetilde{u}_j} - \overline{\widetilde{u}_i \widetilde{u}_j} = T_{ij} - \overline{\tau}_{ij} \tag{6}$$

where L_{ij} is the resolved stress tensor and T_{ij} is the subgrid stress tensor, at the test filter scale. For more details in the dynamic Smagorinsky SGS the reader is referred to Germano et. al [9]. The structural computations are carried out using the finite-element method.

III. Results and Discussion

Figure 2 shows the pressure field for three different angle of attach and two different Mach numbers. The analysis of the pressure field reveals that the stagnation point is located below the leading-edge, on the lower surface of the wing. The increase of the Mach number causes an increase of the pressure on the lower surface, pressure side. Pressure waves radiating from the lower surface of the wing are observed as well. The magnitude of the pressure waves increase also increase with the Mach number. The time-dependent pressure fluctuations, at the surface of the wing, causes a time-dependent lift coefficient, as shown in Figure 3.

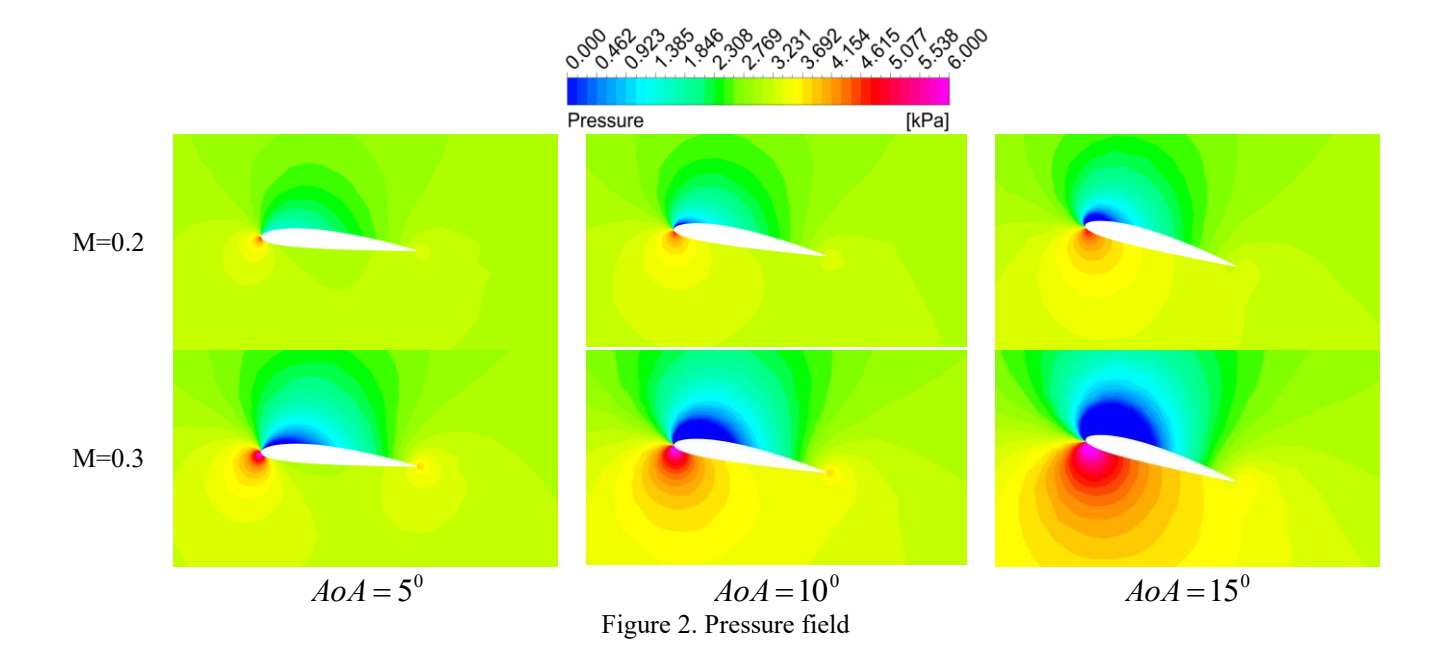


Figure 3 shows the time-dependent lift coefficient. The analysis of the lift coefficient reveals large fluctuations. It is expected that the fluctuations of the time-dependent lift coefficient are reflected onto the structural stresses.

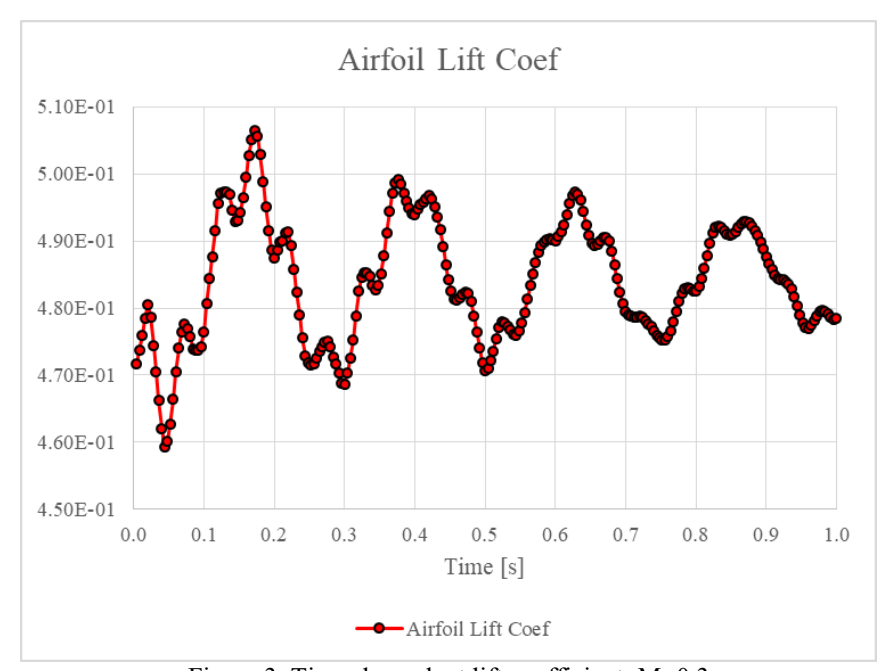


Figure 3. Time-dependent lift coefficient; M=0.3

Figure 4 presents the time-dependent drag coefficient. The analysis of the time-dependent drag coefficient reveals the presence of large fluctuations, as in the case of lift coefficient.

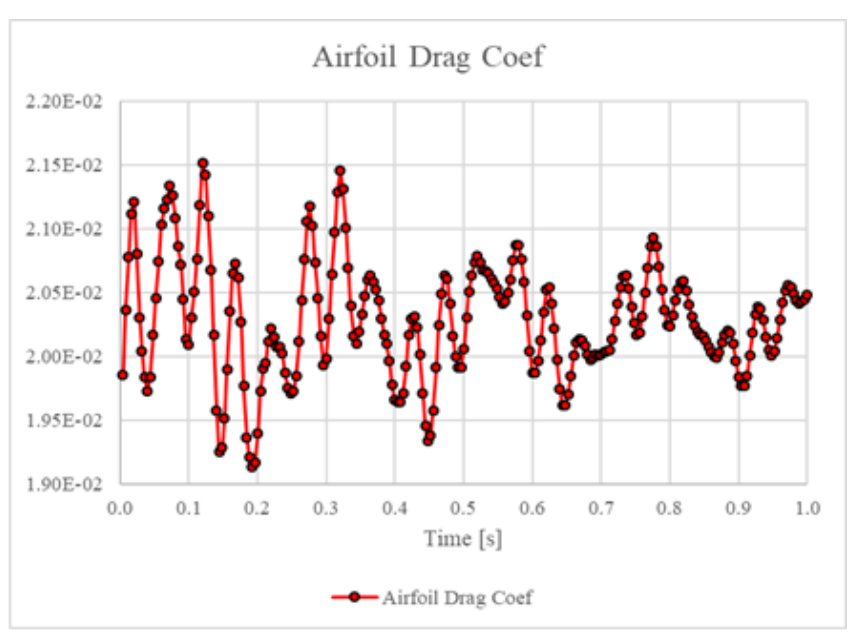


Figure 4. Time-dependent drag coefficient; M=0.3

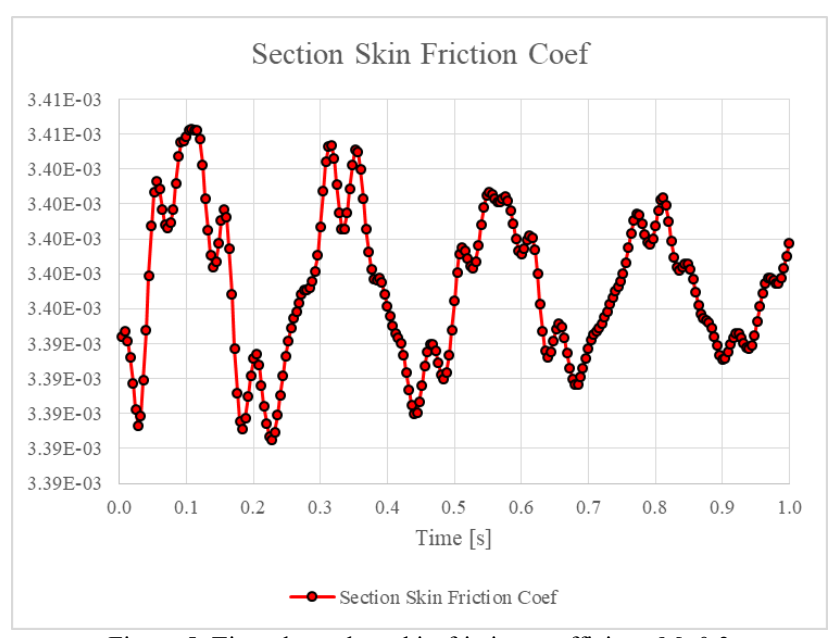


Figure 5. Time-dependent skin-friction coefficient; M=0.3

Figure 5 presents the time-dependent skin-friction coefficient. The analysis reveals that in spite of the fluctuations of the skin-friction the flow remains attached. Figure 6 presents the time-dependent elastic deformation, for M=0.3. The analysis reveals the presence of relatively large deformations, which attenuates in time.

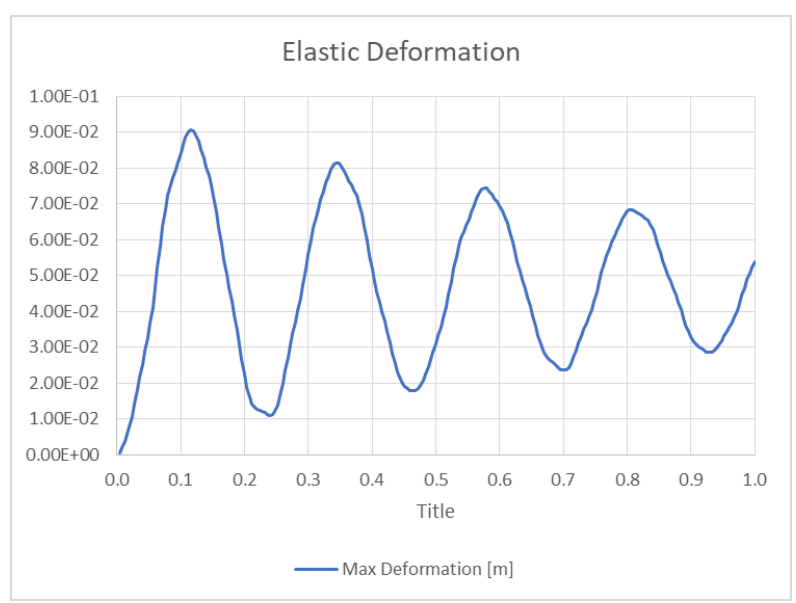


Figure 6. Time-dependent elastic deformation of the fixed wing; M=0.3

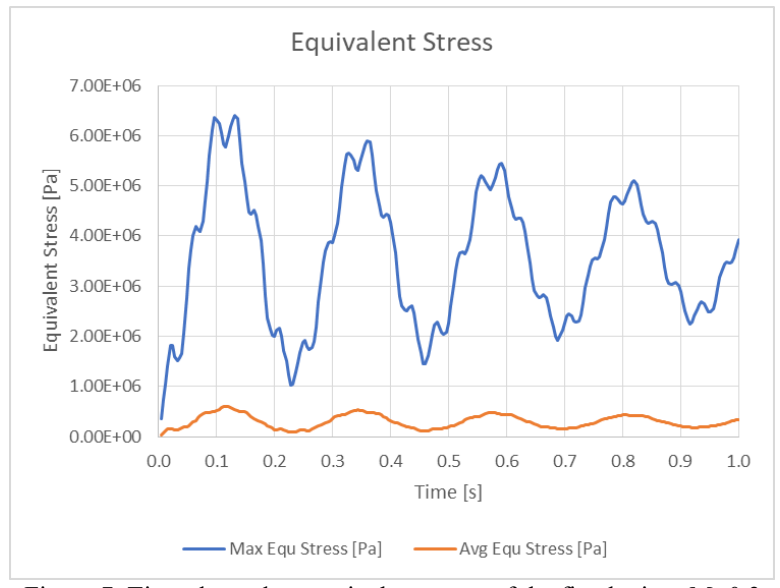


Figure 7. Time-dependent equivalent stress of the fixed wing; M=0.3

Figure 7 presents the time-dependent equivalent stress, for M=0.3. The time-dependent equivalent stress follows a similar trend with the elastic deformation. The present research reveals that the wing's deformation increases with the increase of the Mach number. Therefore, Figure 8 shows the comparison of the time-dependent elastic deformation for three different Mach numbers. Overall, the magnitude of the elastic deformations increase with the Mach number.

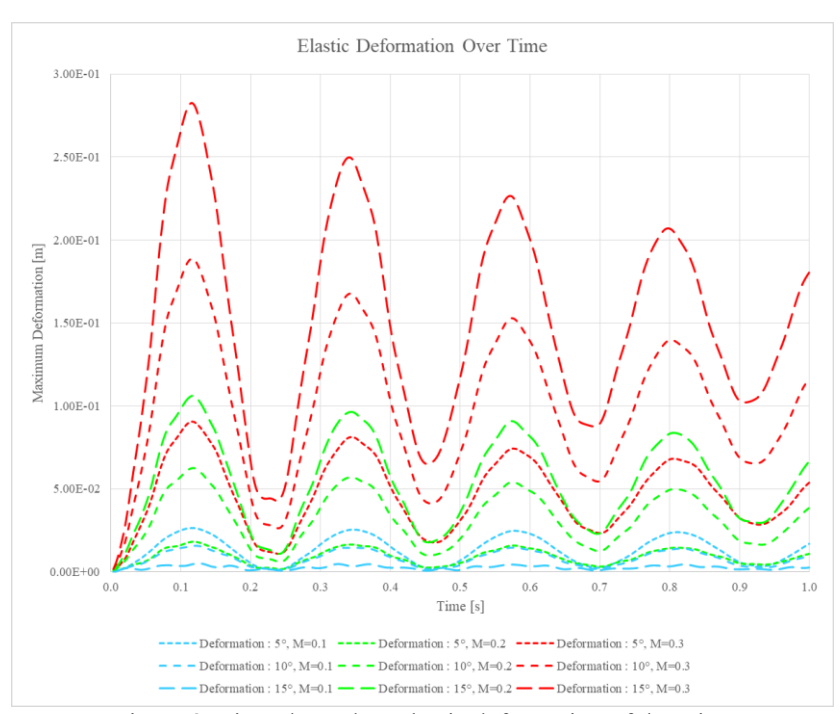


Figure 8. Time-dependent elastic deformation of the wing

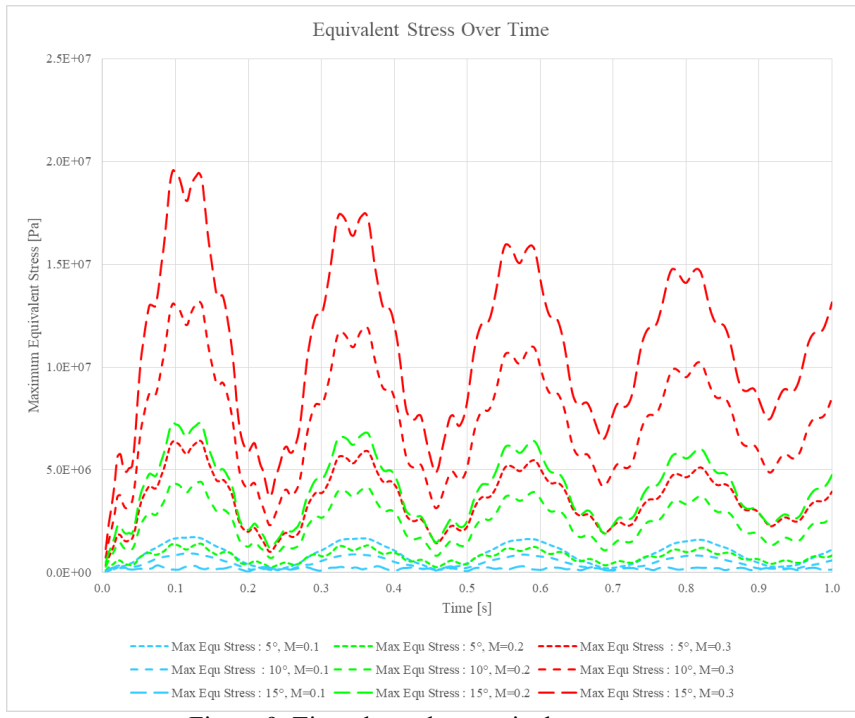


Figure 9. Time-dependent equivalent stresses

Figure 9 presents the comparison of the time-dependent equivalent stress for three different Mach numbers. Similar to the elastic deformations, the equivalent stresses increase with the Mach number.

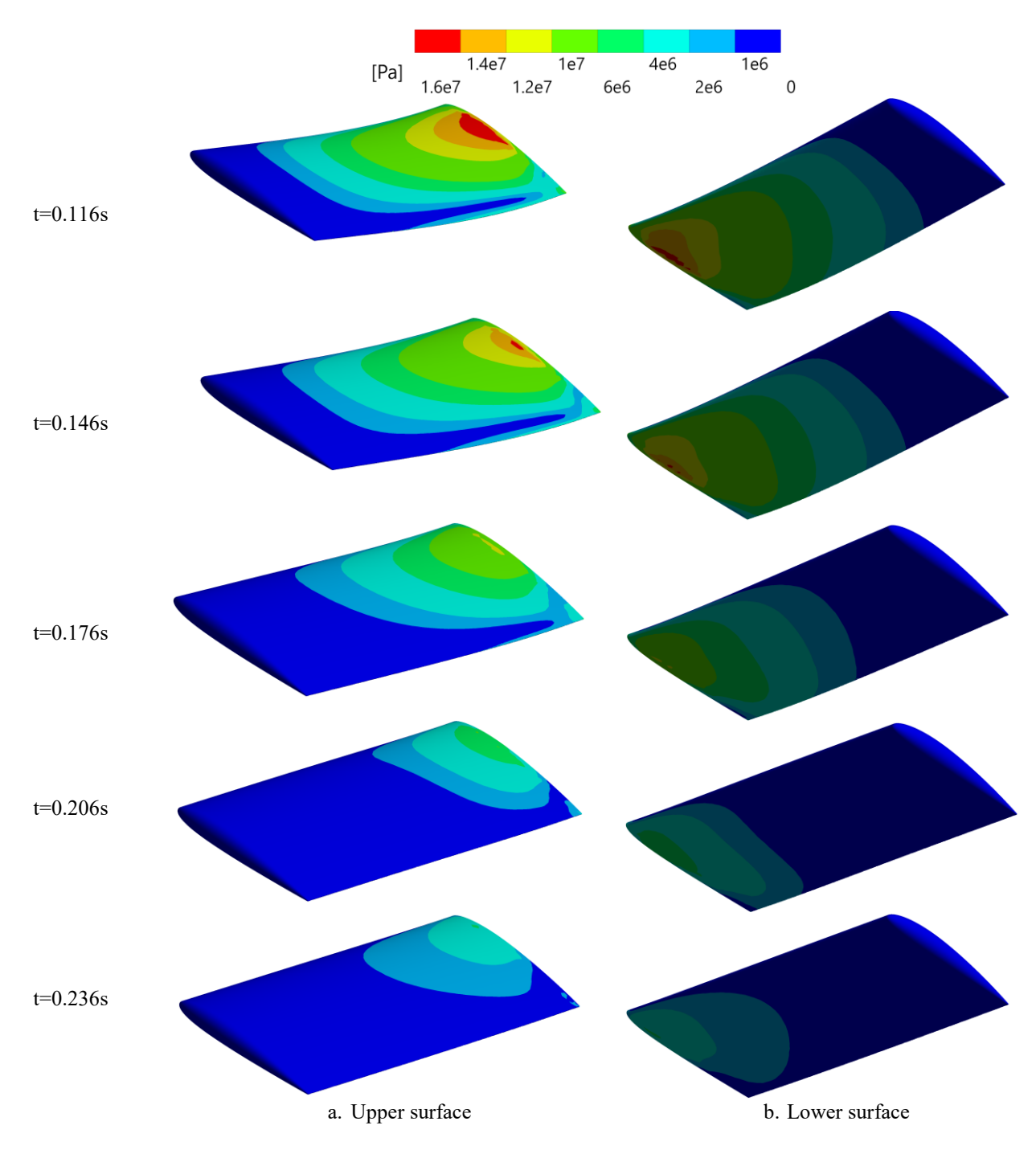


Figure 10. Equivalent stresses of the fixed wing at M=0.3

Figure 10 presents the equivalent stresses for the upper and lower surfaces, for M=0.3. The analysis shows that the upper surface experiences higher stresses in the hub region while the lower surface exhibits higher stresses at the tip of the wing.

IV. Conclusions

Mach number effect on the aeroelasticity phenomena, of fixed wings, is computationally studied using a fully-coupled aeroelastic approach. The flow field is computed using the CFD approach using finite-differences, while the structural analysis is performed using the finite-element method. The study shows that the pressure on the lower surface of the wing increases with the Mach number. The elastic deformation and stresses, on the wing, increase with the Mach number. The analysis shows that the upper and lower surfaces of the wing experience alternatively, tensions and compressions.

References

¹Papadakis, M., Nizampatnam L., and Hoffmann, K., "Computational Investigation of Blade Vortex Interaction Noise", AIAA Paper 99-0231, 38th Aerospace Sciences Meeting and Exhibit, Reno (NV), Jan. 10-13, 2000.

²Singer B.A., Brentner K.S., Lockard D.P. and Lilley G.M. "Simulation of Acoustic Scattering from a Trailing Edge", AIAA Paper 99-0231, 37th Aerospace Sciences Meeting and Exhibit, Reno (NV), Jan. 12-15, 1999.

³Singer B.A., Lockard D.P., Brentner K.S. "Computational Aeroacoustic Analysis of Slat Trailing- Edge Flow", AIAA Journal, Vol. 38, No. 9, pp. 1558-1564, September, 2000.

⁴Abelló, J. C., and George, A.R., "Rotorcraft BVI Noise Reduction by Attitude Modification," paper presented at the 5th AIAA/CEAS Aeroacoustics Conference, Bellevue, Washington, May, 10-12, 1999

⁵Abello, J., George, A., Wake Displacement Study of Attitude and Flight Parameter Modifications to Reduce Rotorcraft Blade-Vortex Interaction (BVI) Noise, AIAA 2003-3174, 9th AIAA/CEAS Aeroacoustics Conference, 12-14 May 2003, Hilton Head, SC

⁶Becker, S., Kaltenbacher, M., Ali, I., Escobar, M., Hahn, C., Sound Generation by Flow around Simple Geometries: Simulation and Experiment, 12th AIAA/CEAS Aeroacoustics Conference, 8-10 May 2006, Cambridge

⁷Felten, F., Lund,T., Numerical Simulation of parallel Airfoil/Vortex Interaction Using a Zonal Hybrid RANS/LES Method, AIAA2005-5127

⁸Nagarajan, S., Lele, S., Prediction of Sound Generated by a Pitching Airfoil: A comparison of RANS and LES, 12th AIAA/CEAS Aeroacoustics Conference, 8-10 May 2006, Cambridge, MA

⁹Wang, M., Moin, P., Computation of Trailing-Edge Flow and Noise Using Large-Eddy Simulation, AIAA Journal, Vol.38, No.12, 2000

¹⁰Magagnato, E., Sorguven, E., Gabi, M., Far Field Prediction by Large Eddy Simulation and Ffowcs -Willimas Hawkings Analogy, AIAA Paper 3206-2003, May 2003

¹¹Lardeau, S., Leschziner, M.A., Unsteady Reynolds–Averaged Navier-Stokes Computations of Transitional Wake/Blade Interaction, AIAA, Vol.42, No.8, 2004, pp. 1559-1571

¹²Bernandini,G., Serafini,J., Gennaretti, M., Aeroelsatic Modeling Effect in Rotor BVI Noise Prediction, 12th AIAA/CEAS Aeroacoustics Conference, 8-10 May 2006, Cambridge, MA

¹³Lyrintzis, A., Xue, Y., Study of Noise Mechanisms of Transonic Blade-Vortex Interactions, AIAA Journal, Vol.29, No.10, 1990, pp.1562-1572

¹⁴Johnson, W., Calculation of Blade-Vortex Interaction Airloads on Helicopter Rotors, Journal of Aircraft , Vol.26, No.5, 1989, pp.470-475

¹⁵Seath, D., Kim, J., Wilson, D., Investigation of Parallel Blade-Vortex Interaction at Low Speed, Journal of Aircraft, Vol.26, No.4, 1989, pp.328-333

¹⁶Oh, W., S., Kim, J.S., Kwon, O.J., Numerical Simulation of Two-Dimensional Blade-Vortex Interactions Using Unstructured Adaptive Meshes, AIAA Journal, Vol. 40., No.3, 2002, pp. 474-480

¹⁷Strawn, R. C., Ahmad, J., Duque, E. P. N, "Rotorcraft Aeroacoustics Computations with Overset Grid CFD Methods," 54th AHS Annual Forum, Washington DC, May 22-24, 1996.

¹⁸Horner, M., Galbraith, R., Coton, F., Examination of Vortex Deformation during Blade-Vortex Interaction, AIAA Journal, Vol.34, No.6, 1996, pp.1188-1194

¹⁹Hu, H., Jordan, L., CFD Investigation of Double Swept Blade in BVI Noise Reduction, 9th AIAA/CEAS Aeroacoustics Conference, 12-14 May 2003, Hilton Head, SC

²⁰Smagorrinsky, J.S., General circulation experiments with the primitive equation, Monthly Weather Rev.91:99-164, 1963

²¹Lilly, D.K., On the application on the eddy viscosity concept in the inertial sub-range of turbulence, NCAR Manuscript, pp195-200, 1996

 $^{22}\mathrm{M}.$ Germano, U. Piomelli, P. Moin, and W. H. Cabot, A dynamic subgrid-scale eddy viscosity model. Phys. Fluids A, 3(7):1760–1765, 1991